ELSEVIER

Journal of Molecular Catalysis A: Chemical 176 (2001) 195–203

JOURNAL OF MOLECULAR CATALYSIS A: CHEMICAL

www.elsevier.com/locate/molcata

A novel catalyst for DME synthesis from CO hydrogenation 1. Activity, structure and surface properties

Gong-Xin Qi, Xiao-Ming Zheng*, Jin-Hua Fei, Zhao-Yin Hou

Institute of Catalysis, Xixi Campus, Zhejiang University, 34 Tianmushan Road, Hangzhou 310028, PR China

Received 9 January 2001; received in revised form 12 April 2001; accepted 30 May 2001

Abstract

The effect of manganese on the dispersion, reduction behavior and active states of surfaces of γ-Al_2O_3 supported copper catalysts was investigated by X-ray powder diffraction (XRD), temperature-programmed reduction (TPR) and XPS technologies. The relationship between the area of metallic copper and the activity of dimethyl ether (DME) synthesis from CO/H_2 was also investigated. The catalytic activity over Cu-MnO_x/γ-Al_2O_3 catalyst for CO hydrogenation is higher than that of Cu/γ-Al_2O_3. The adding of manganese increases the dispersion of the supported copper oxide. For the CuO/γ-Al_2O_3 catalyst, there are two reducible copper oxide species; α- and β-peaks are attributed to the reduction of highly dispersed copper oxide species and bulk CuO species, respectively. For the CuO-MnO_x/γ-Al_2O_3 catalyst, four reduction peaks are observed. The α-peak is attributed to the reduction of high dispersed copper oxide species; β-peak is ascribed to the reduction of bulk CuO; γ-peak is ascribed to the high-dispersed CuO interacting with Mn; and δ-peak is attributed to the reduction of the manganese oxide interacting with copper oxide. XPS results showed that Cu^+ mostly existed on the working surface of the Cu-Mn/γ-Al_2O_3 catalysts. Cu promoted the catalytic activity with positive charge, which was formed by means of long path exchange function between Cu–O–Mn. These results indicate that there are synergistic interactions between the copper and manganese oxide, which are responsible for the high activity of CO hydrogenation.

Keywords: DME synthesis; Cu-Mn catalyst; CO hydrogenation

1. Introduction

Dimethyl ether (DME) is an important chemical for the production of gasoline, ethylene, aromatics and other chemicals [1–4]. Its applications as a fuel or a fuel additive for vehicles and family cooking have been studied [5–7]. In view of the environmental protection, the substitution of DME for freon as an aerosol spray [8] and a refrigerant [9] is being considered.

At present time, almost all-commercial DME were produced by the dehydration of methanol using acidic porous materials such as zeolites, sillica–alumina, alumina etc. as the catalyst [10] (Eq. (1)), while methanol can be produced from CO/H_2.

$$2CH_3OH \rightarrow CH_3OCH_3 + H_2O \quad (1)$$

It is reported that DME can be synthesized from CO/H_2 in a single step (Eqs. (2) and (3)). It is much more thermodynamically and economically favorable [11–13].

* Corresponding author. Tel.: +86-571-8273417; fax: +86-571-8273283.
E-mail address: cuihua@dial.zju.edu.cn (X.-M. Zheng).

1381-1169/01/$ – see front matter
PII: S1381-1169(01)00257-6

$$2CO + 4H_2 \rightarrow CH_3OCH_3 + H_2O, \quad \Delta H = -207.382\,kJ/mol \tag{2}$$

$$3CO + 3H_2 \rightarrow CH_3OCH_3 + CO_2, \quad \Delta H = -247.468\,kJ/mol \tag{3}$$

In early 1990s, most researches focused on DME synthesis in a slurry reactor in the presence of dual catalyst systems consisting of a methanol-synthesis catalyst (composed of CuO, ZnO, Al_2O_3) and a methanol dehydration catalyst (γ-Al_2O_3 or zeolites) [1,11,14]. At the same time, there are quite a few patents describing the method of DME synthesis directly from synthesis gas in a fixed-bed reactor [15–24]. The typical procedure in these patents is as follows: CO/H_2 passed over a hybrid catalyst consisted of a methanol synthesis catalyst and a dehydration catalyst at 240–300°C, 3.0–6.0 MPa, and GHSV = 500–5000 h^{-1}. The catalysts employed in this process are methanol synthesis catalysts (Cu-Zn, Zn-Cr, Cu-Zn-Al, Cu-Zn-Cr, etc.) mixed with the dehydration catalyst(γ-Al_2O_3 or zeolites).

We have developed a new catalyst system Cu-MnO_x/γ-Al_2O_3 prepared by a simple impregnation method [25]. By using this catalyst, the reaction can be carried out at a lower pressure with high CO conversion and high selectivity of DME. In this paper, the effect of manganese on the dispersion of Cu, reduction behavior of catalysts and active state of γ-alumina supported CuO catalysts was investigated by means of the temperature-programmed reduction (TPR), X-ray powder diffraction (XRD) and XPS techniques.

2. Experimental

2.1. Catalysts preparation

The catalysts were prepared by the conventional wet impregnation method with $Cu(NO_3)_2$, $Mn(NO_3)_2$, mixed aqueous solution taken in appropriate ratio (Cu:Mn). The support was γ-Al_2O_3, 20–40 mesh. The catalysts were dried at 120°C followed by calcination in air stream for a certain time. The individual and mixed catalysts are denoted as xCu/γ-Al_2O_3, yMn/γ-Al_2O_3 or xCu-yMn/γ-Al_2O_3, where x and y denote the loading of metallic copper and manganese (mmol) per gram support.

2.2. Catalytic reaction

Catalytic activity measurements were carried out by using high pressure micro reactor (MRC8004, i.d. = 8 mm) after introducing pretreatment gas (H_2) at 300°C for 3 h, the reactant gas (n(CO)/(H_2) = 2/3) was passed through the catalyst bed (2 ml, 20–40 mesh) under a total pressure of 2.0 MPa and a space velocity of 1800 h^{-1}, at temperature of 220–300°C. The tubing from the catalyst bed to the gas chromatograph was heated at 100–150°C so as to avoid any condensation of the products. All experimental data were obtained under steady-state conditions that were usually maintained for several hours. The products were analyzed by on-line gas chromatograph with a thermal detector, in which columns Porapak-Q was used to separate reaction products.

2.3. Catalyst characterization

Measurement of XRD was conducted by using a Rigaku D/Max-B for analysis of the crystal phase. Cu Kα radiation. The specific surface area of metallic copper was measured by the decomposition of N_2O [26–28] on the surface of metallic copper as follows: $2Cu + N_2O = N_2 + (Cu–O–Cu)_s$. The pulse titration technique was employed in our experiment. N_2 was used as the carrier gas and a thermal conduct detector was used to detect the amount of the consumption of N_2O. The specific area of metallic copper was calculated assuming a reaction stoichiometry of two Cu atoms per oxygen atom and a Cu surface density of 1.46×10^{19} Cu atoms/m^2 [26,28].

2.4. Temperature-programmed reduction of hydrogen (H_2-TPR)

TPR measurements were made in a flow system. Twenty milligrams of catalyst was pretreated in air at 400°C and placed in a TPR cell at room temperature, after that H_2–N_2 (5:95) gas was introduced. The water produced by the reduction was trapped on a 5A molecular sieve. The temperature of the sample was programmed to rise at a constant rate of 10°C/min and the amount of H_2 uptake during the reduction was measured by a thermal conductivity detector (TCD).

2.5. Measurement of photoelectron spectra

Measurement of photoelectron spectra was conducted by using a VG-ESCALAB MKIII surface analyzer, Al Kα, reference to the C 1s level at 285.0 eV.

3. Results and discussion

3.1. Effect of composition of the catalyst on the catalytic activity

Fig. 1 shows the influence of Cu loading amount of Cu/γ-Al_2O_3 catalyst upon the syngas to DME (STD) process, which was carried out at 2.0 MPa and GHSV = 1800 h^{-1} based on the gross catalyst volume. From Fig. 1, it can be seen that the activity of Cu/γ-Al_2O_3 catalysts increases with Cu loading from 0.5 to 2 mmol/g support and then decreases from a higher loading of metallic Cu. From Fig. 1, it can be found that the optimized Cu loading is 2 mmol/g support.

The result of CO hydrogenation over Cu-Mn/γ-Al_2O_3 catalyst. was shown in Fig. 2, which exhibited that Mn addition showed a marked improvement in the activity of catalysts, particularly, the conversion of CO. In addition, the catalytic activity of the Cu-Mn/γ-Al_2O_3 catalysts increased with the increase of Mn/Cu ratio until it reached a maximum at Mn/Cu ratio of 1.

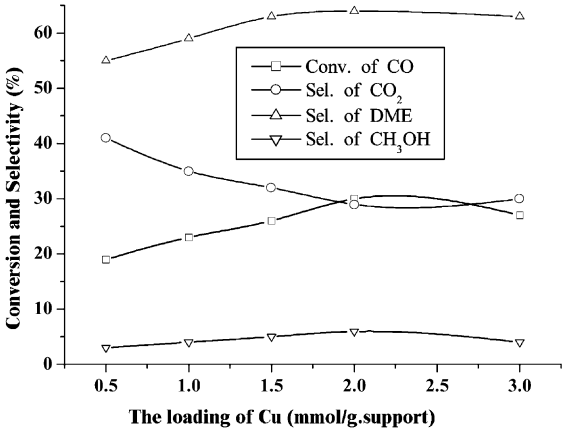

Fig. 1. The effect of the loading of Cu on the activity of CO hydrogenation. Reaction condition: $T = 260°C$; GHSV = 1800 h^{-1}; $CO/H_2 = 2/3$.

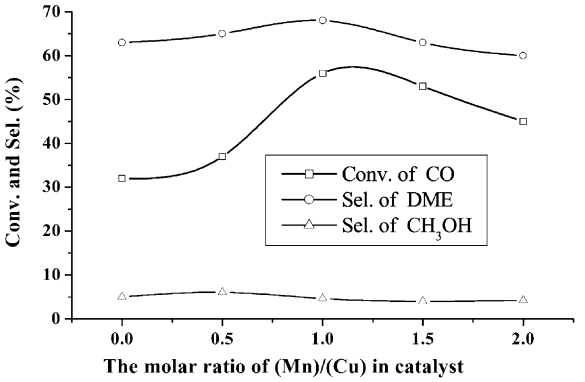

Fig. 2. The effect of *n*(Mn)/*n*(Cu) ratio on the activity for CO hydrogenation. Reaction condition: $T = 260°C$; $P = 2.0$ MPa; GHSV = 1800 h^{-1}; $CO/H_2 = 2/3$.

Various composition and different preparation methods of Cu-containing catalysts can strongly influence their catalytic activity for methanol synthesis. It has been proposed that [29–32] the yield of methanol is directly proportional to the surface of metallic copper for Cu/ZnO/Al_2O_3 or supported copper catalysts in the synthesis of methanol from the hydrogenation of CO/CO_2. However, there are also conflicting reports [33–35] which suggest that the yield of methanol is not proportional to the surface area of metallic copper for the Cu/ZnO and Cu/ZnO/Al_2O_3 catalysts. There are few studies on the relations between the catalytic activity for DME synthesis from CO hydrogenation and the surface area of metallic copper.

In our experiment, the effect of the surface area of metallic copper on the activity of DME synthesis from the CO hydrogenation results was shown in Fig. 3. It can be seen that the catalytic activity increased with the increase of the surface area of metallic copper, but it was not a linear relationship. This indicates that the catalytic activity of the catalysts depends on both the metallic copper surface area and the powerful synergy between copper and manganese oxide.

3.2. XRD phase analyses of calcined catalysts

Fig. 4 shows the XRD profiles of CuO/γ-Al_2O_3 catalysts with different Cu content. From Fig. 4, at low Cu loading (<1 mmol) no visible CuO crystal phases can be observed; as the CuO loading increasing, the crystal phase of CuO becomes apparent.

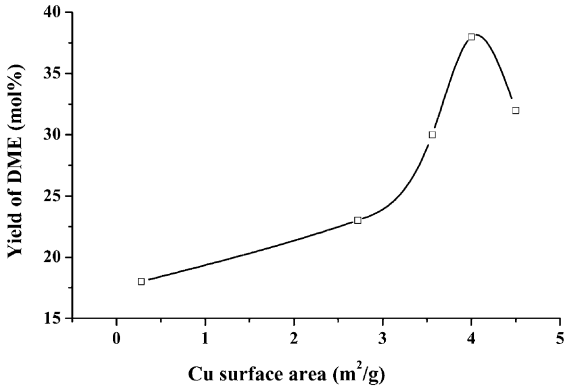

Fig. 3. Relationship between the yield of DME and surface area of Cu. Reaction condition: $T = 260^{\circ}C$; $P = 2.0\,MPa$; $GHSV = 1800\,h^{-1}$; $CO/H_2 = 2/3$.

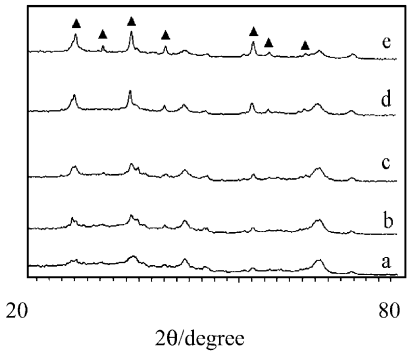

Fig. 5. XRD profiles of MnO_x/γ-Al_2O_3 catalysts with different Mn loading: (a) 0.25Mn/γ-Al_2O_3; (b) 0.5Mn/γ-Al_2O_3; (c) 1.0Mn/γ-Al_2O_3; (d) 2.0Mn/γ-Al_2O_3; (e) 4.0Mn/γ-Al_2O_3. MnO_2 (▲).

Fig. 5 shows the XRD profiles of MnO_x/γ-Al_2O_3 catalysts with different Mn content. At low Mn loading (<0.25 mmol) no visible MnO_2 crystal phase can be observed. As the Mn loading increased, the crystal phase of MnO_2 becomes obvious. Fig. 6 shows the XRD profiles of CuO-MnO_x/γ-Al_2O_3 catalysts with different Mn content. XRD (Fig. 6) results show that MnO_x component in Cu-MnO_x/γ-Al_2O_3 catalysts is high dispersed, its XRD peaks are not observed; other component in Cu-MnO_x/γ-Al_2O_3 catalysts are more dispersed than that in CuO/γ-Al_2O_3 catalysts. As the adding of Mn increasing, the CuO peaks get lower and lower indicating that CuO dispersed more and more. The results indicate that the adding of Mn enhances the dispersion of CuO, which is consistent with the results of active area, particle size of metallic copper and dispersion of Cu (Table 1). This indicates that there may be an interaction between copper oxide and manganese oxide particles, which restrains phase transformation of CuO and MnO_2. From the Figs. 4 and 6, it can be seen that the adding of manganese enhances the dispersion of CuO, while the existence of copper also enhances the dispersion of manganese oxide.

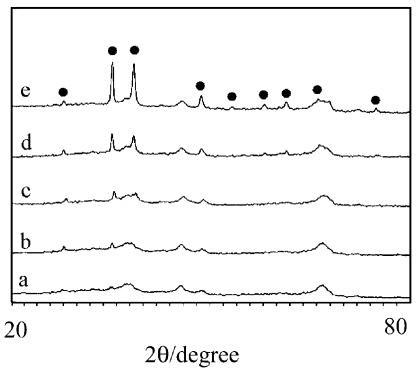

Fig. 4. XRD profiles of CuO/γ-Al_2O_3 catalysts with different Cu loading: (a) 0.5Cu/γ-Al_2O_3; (b) 1.0Cu/γ-Al_2O_3; (c) 1.5Cu/γ-Al_2O; (d) 2.0Cu/γ-Al_2O_3; (e) 3.0Cu/γ-Al_2O_3. CuO (●).

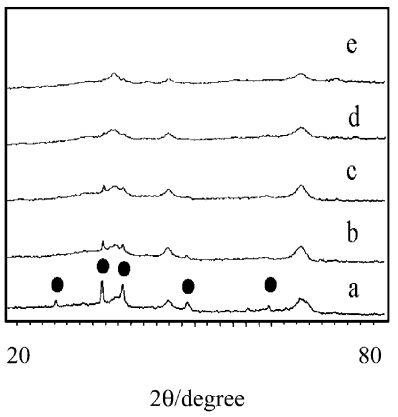

Fig. 6. XRD profiles of CuO/γ-Al_2O_3 catalysts with different Mn loading: (a) 2.0Cu/γ-Al_2O_3; (b) 2.0Cu-0.5Mn/γ-Al_2O_3; (c) 2.0Cu-1.0Mn/γ-Al_2O_3; (d) 2.0Cu-2.0Mn/γ-Al_2O_3; (e) 2.0Cu-4.0Mn/γ-Al_2O_3. CuO (●).

Table 1
Properties of catalysts

Catalysts	Particles size (nm)	Active area (m^2/g cat)	Dispersion (%)
2.0Cu/γ-Al_2O_3	52	0.28	0.12
2.0Cu-0.5Mn/γ-Al_2O_3	7.6	2.72	1.13
2.0Cu-1.0Mn/γ-Al_2O_3	5.8	3.56	1.48
2.0Cu-2.0Mn/γ-Al_2O_3	4.7	4.40	1.70
2.0Cu-4.0Mn/γ-Al_2O_3	5.2	4.00	1.60

3.3. XRD analyses of reduced catalysts

When the CuO/γ-Al_2O_3, CuO-MnO_x/γ-Al_2O_3 catalysts were reduced by H_2 at 300°C, it can be found that XRD (Fig. 7) lines for CuO were absent for the reduced sample while diffraction lines for Cu were present. This indicates that CuO in the catalysts was completely reduced to metallic copper. The mean crystallite sizes were determined by the Scherrer equation, $d = \kappa\lambda/\cos\theta$, and the results are listed in Table 1. This shows that the mean crystallite size of metallic copper in Cu-Mn/γ-Al_2O_3 is much smaller than that in CuO/γ-Al_2O_3 and decreases with the increasing manganese content until the ratio of n(Mn)/n(Cu) is 1. The mean particle sizes of metallic copper determined by X-ray diffraction are consistent with those calculated by specific area of metallic copper (see Table 1). The diffraction line of Cu is broadened, suggesting that Cu atoms were high dispersed and exhibited "X-ray amorphous" features due to the formation of amorphous and/or microcrystallines during reduction. Klier and co-workers [36,37] have also observed the broadening or the absence of X-ray diffraction lines for Cu and suggested that Cu was highly dispersed and a considerable amount of amorphous phase was found. It is consistent with our observations.

3.4. H_2-TPR of CuO/γ-Al_2O_3 catalysts

With increasing copper loading, two TPR peaks, namely α and β as shown in Fig. 8, can be observed in the TPR patterns. The area of β-peak obviously increases with increasing the copper loading, but the area of α-peak has a maximum value occurring at 2 mmol Cu/g support, when the copper loading is lower than 2 mmol Cu, the β-peak area is smaller than that of α-peak, and when the copper loading is higher than 2 mmol Cu, the β-peak area is larger than that of α-peak and the α-peak becomes a shoulder. In addition, the overlap of α- and β-peaks becomes very

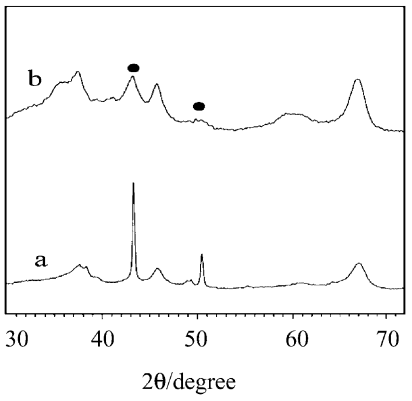

Fig. 7. XRD profiles of reduced 2.0Cu/γ-Al_2O_3 and 2.0Cu-2.0Mn/γ-Al_2O_3: (a) 2.0Cu/γ-Al_2O_3; (b) 2.0Cu-2.0Mn/γ-Al_2O_3. Cu (●).

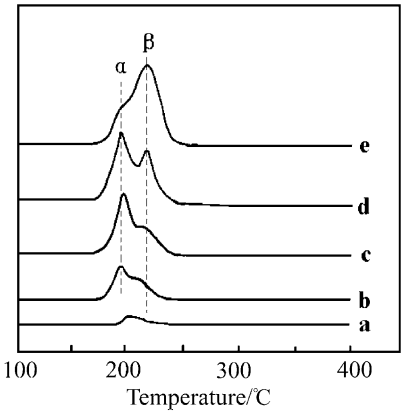

Fig. 8. The TPR profiles of CuO/γ-Al_2O_3 catalysts with different Cu loading: (a) 0.5 mmol; (b) 1.0 mmol; (c) 1.5 mmol; (d) 2.0 mmol; (e) 3.0 mmol.

serious when copper loading is higher than 3 mmol Cu/g support. It seems to have a saturated phenomenon occurring at 2.0 mmol Cu/g support for α-peak. The serious overlap of α- and β-peaks implies that the reducibility of these two types of copper oxide species gradually approaches to the same.

Combining the results of TPR and XRD, it can be found that the higher the copper loading, larger the β-peak area of TPR and the larger the signal intensity of XRD (Fig. 4). There is a maximum area of α-peak when the loading of Cu is 2 mmol/g support. These strongly suggest that the β-peak copper oxide species belong to the bulk CuO and the α-peak copper oxide species is contributed to the dispersed CuO.

Friedman et al. [38] reported that for $CuO/\gamma\text{-}Al_2O_3$ catalysts, saturation of the support surface occurs at a copper loading approximately 4–5 wt.% Cu per 100 m^2/g Al_2O_3. Above the threshold loading, formation of crystalline CuO is observed. According to Friedman's saturation value, 'monolayer' coverage of supported employed in this study (BET area = 230 m^2) should occur at a copper content of approximately 2 mmol/g support, which is compatible with the TPR results. Hence, α- and β-peaks can be unambiguously attributed to the reduction of highly dispersed copper oxide species and bulk-like CuO, respectively.

3.5. H_2-TPR of $CuO\text{-}MnO_x/\gamma\text{-}Al_2O_3$ catalysts

The reduction profile (Fig. 9) of $MnO_x/\gamma\text{-}Al_2O_3$ is characterized by two prominent peaks, at 320 and 370°C, respectively. The lower temperature peak attributes to the reduction of MnO_2 to Mn_3O_4; the high temperature peak attributes to the reduction of Mn_3O_4 to MnO [39]. For the thermodynamic reasons, further reduction of MnO does not occur under the applied experimental conditions. This result is consistent with Wollner's conclusion [39].

The TPR profiles of the mixed compounds were also shown in Fig. 9. From Fig. 9, it can be seen that the reduction position of $CuO\text{-}MnO_x/\gamma\text{-}Al_2O_3$ catalysts lies in between the $CuO/\gamma\text{-}Al_2O_3$ and the $MnO_x/\gamma\text{-}Al_2O_3$. Apparently, the presence of copper enhances the reduction of manganese oxide because of hydrogenation spillover [39].

From Fig. 9, it can be also seen that when the manganese loading is lower than 0.25 mmol/g support,

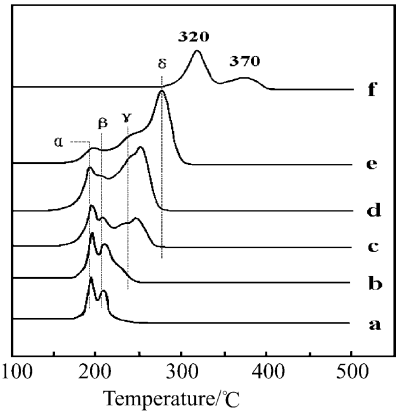

Fig. 9. TPR profiles of $CuO/\gamma\text{-}Al_2O_3$ with various Mn loading: (a) $2.0Cu/\gamma\text{-}Al_2O_3$; (b) $2.0Cu\text{-}0.5Mn/\gamma\text{-}Al_2O_3$; (c) $2.0Cu\text{-}1.0Mn/\gamma\text{-}Al_2O_3$; (d) $2.0Cu\text{-}2.0Mn/\gamma\text{-}Al_2O_3$; (e) $2.0Cu\text{-}4.0Mn/\gamma\text{-}Al_2O_3$; (f) $2.0Mn/\gamma\text{-}Al_2O_3$.

three peaks are observed and when the manganese loading is higher than 0.25 mmol/g support four peaks are observed. The four peaks are designated by α, β, γ, δ in Fig. 9. The position of α- and β-peaks remain unchanged with increasing manganese loading. The intensities of α- and β-peaks decrease rapidly with the increase of manganese loading from 0.25 to 4.0 mmol/g support. The XRD results (Fig. 6) show that as the adding of manganese increasing, the CuO peaks get lower and lower. Compared to TPR results of $CuO/\gamma\text{-}Al_2O_3$ (Fig. 8) we propose that α- and β-peaks are contributed to the high dispersed CuO and bulk CuO species, respectively.

From Fig. 9, it can be seen that the position of γ-peak remains unchanged with increasing manganese loading, while, the intensity of γ-peak increases with the increasing manganese loading. We propose that the γ species is ascribed to the high-dispersed CuO interacting with Mn. The area of δ-peak monotonously increases with increasing manganese loading and shifts to higher temperature. On the basis of XRD results and these findings, it is concluded that the peak δ may be ascribed to the reduction of manganese oxide interacting with copper oxide. The TPR results show that there exists interaction between the copper and manganese oxide, which causes TPR peaks of the $CuO\text{-}MnO_x/\gamma\text{-}Al_2O_3$ catalyst different from the individual supported copper and manganese oxide catalysts.

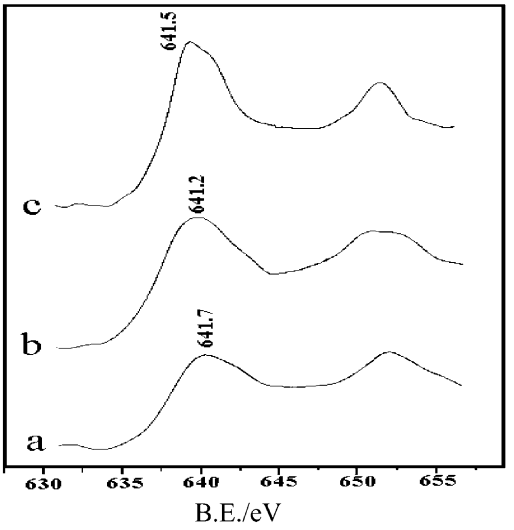

Fig. 10. XPS Mn 2p spectra of 2.0Cu-2.0Mn/γ-Al_2O_3: (a) before reduction; (b) after reduction; (c) after reaction.

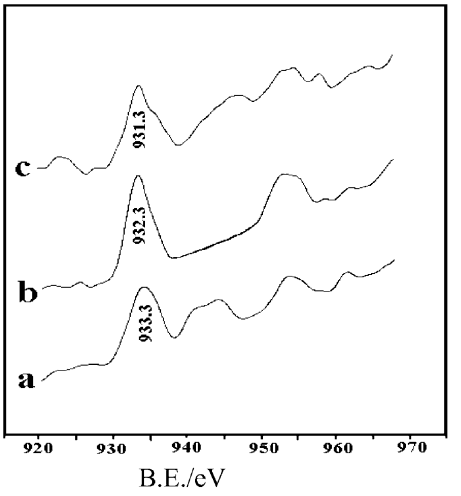

Fig. 11. XPS Cu 2p spectra of the 2.0Cu-2.0Mn/γ-Al_2O_3 catalyst: (a) before reduction; (b) after reduction; (c) after reaction.

3.6. Surface state of activity

The XPS of the Mn 2p level for the before reduced, after reduced and used catalysts are shown in Fig. 10. From Fig. 10, it can be seen that the binding energy (BE) of the Mn 2p level for the calcined catalyst was very close to that for pure Mn_2O_3 (BE = 642 eV). On the other hand, in the reduced catalyst, the BE value of the Mn 2p band was decreased, which is contributed to the MnO. For the used catalyst, it is found that there exists two kinds of manganese species; one shows a BE of 641.5 eV and another a BE of 642 eV, the latter species contributes to MnO_2. Based on the results mentioned above, it is concluded that the valence of Mn is +2 after reduction, while it increases to +3 and +4 after reaction.

The XPS of the Cu 2p level for the before reduced, after reduced and used catalysts are shown in Fig. 11. From Fig. 11, it can be seen that the BE of the Cu 2p level for the before reduced catalyst was very close to that for pure CuO (BE = 933.3 eV). In the reduced catalyst, the BE value of the Cu 2p band was decreased to 932.3 eV, which contributed to the metallic copper. For the used catalyst, the XPS of Cu 2p is 931.3, moreover, a shoulder peak (BE = 933.5 eV) appears which is ascribed to the Cu^{2+}. The former specie is contributed to Cu^{+}. From the Fig. 11, it is concluded that the valence of Cu increases from zero in the reduced catalysts to +1 and +2 in the used catalysts.

The XPS of Cu 2p for the before reduced, after reduced and used 2.0Cu/γ-Al_2O_3 catalyst are shown in Fig. 12. From Fig. 12, it can be seen that the BE of the Cu 2p level for the before reduced catalyst was

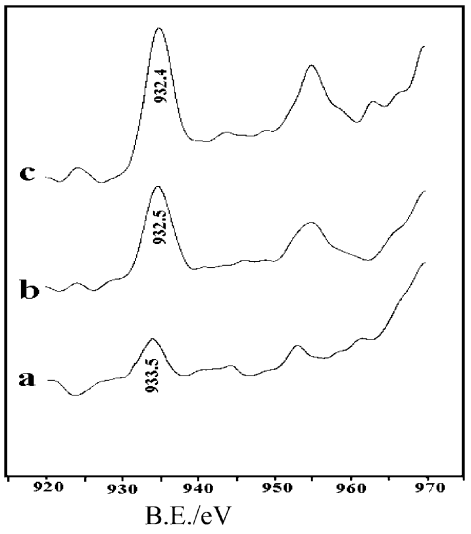

Fig. 12. XPS of Cu 2p for the 2.0Cu/γ-Al_2O_3 catalyst: (a) before reduction; (b) after reduction; (c) after reaction.

very close to that for pure CuO (BE = 933.3 eV). In the reduced catalyst, the BE value of the Cu 2p band was decreased to 932.5 eV, which contributed to the metallic copper. For the used catalyst, the XPS of Cu 2p is 932.4 which is very close to the BE of Cu. From Figs. 10–12, it can be seen that Cu^+ mostly existed on the working surface of the used Cu-Mn/γ-Al_2O_3 catalysts, while, Cu existed on the Cu/γ-Al_2O_3 catalyst. The catalytic activity of CO hydrogenation over CuO-Mn/γ-Al_2O_3 catalyst is higher than that of CuO/γ-Al_2O_3. So it can be concluded that the catalytic activity was promoted by Cu with part of positive charge, which was formed by means of long path exchange function between Cu–O–Mn, which is consistent with many other author's conclusions [40–42].

4. Conclusions

In this paper, the effect of manganese on the dispersion, reduction behavior and active states of surface of supported copper oxide catalysts has been investigated by XRD, TPR and XPS technologies. The catalytic activity over CuO-MnO_x/γ-Al_2O_3 catalyst for CO hydrogenation is higher than that of CuO/γ-Al_2O_3. The activity of DME synthesis from CO/H_2 increases with the increasing the area of metallic copper, but it is not a linear relationship. XRD result shows that the addition of manganese is beneficial in enhancing the dispersion of the supported copper oxide. The TPR results show that there exists strong interaction between the copper and manganese oxide. XPS results show that Cu^+ mostly existed on the working surface of the Cu-Mn/γ-Al_2O_3 catalysts, while, for the Cu/γ-Al_2O_3 catalyst, Cu mostly existed on the working surface. Cu promoted the catalytic activity with positive charge, which was formed by means of long path exchange function between Cu–O–Mn. These results indicate that there is synergistic interaction between the copper and manganese oxide, which is responsible for the high activity of CO hydrogenation.

Acknowledgements

The Zhejiang provincial Natural Science Foundation of China supported this research project.

References

[1] D.M. Brown, B.L. Bhatt, T.H. Hsiung, Catal. Today 8 (1991) 279.
[2] I. Katsumi, Y. Gosei, Kagaku Kyokaishi 40 (1982) 851 (in Japanese).
[3] M.Q. Kang, Z.X. Ren, Hecheng Huaxue 2 (1994) 335 (in Chinese).
[4] Z.-Y. Hou, J.-H. Fei, X.-M. Zheng, Petrochem. Techn. 28 (1999) 64 (in Chinese).
[5] T. Fleisch, C. McCarthy, A. Basu, Alternative Fuels and Exhaust Emissions SAE Special Publications 950061, SAE, Warrendale, USA, 1995, p. 39.
[6] S.C. Sorenson, S.E. Mikkelesen, J.E.T.I. 43 (10) (1995) 57 (in Japanese).
[7] Z.-H. Chen, Y.-Q. Niu, Coal Conversion 19 (1996) 37 (in Chinese).
[8] B. Herman, Aerosol Spray Rep. 33 (1994) 385.
[9] B.H. Minor, T.E. Chisolm, G.S. Shealy, US Patent 5,480,572 (1996).
[10] J.J. Spivey, Chem. Eng. Commun. 110 (1994) 123.
[11] M.R. Gogate, S. Lee, C.J. Kulik, Fuel Sci. Technol. Int. 10 (1990) 281.
[12] S. Lee, M.R. Gogate, C.J. Kulik, Fuel Sci. Technol. Int. 13 (1995) 1039.
[13] J.-L. Li, X.-G. Zhang, T. Inui, Appl. Catal. A: Gen. 147 (1996) 23.
[14] M.R. Gogate, S. Lee, C.J. Kulik, Prepr. Pap. Am. Chem. Soc. Div. Fuel Chem. 38 (1993) 1100.
[15] C. D. Chang, W.K. Bell, US Patent 4,423,155 (1983).
[16] C.D. Chang, A.J. Silvestri, US Patent 3,894,102 (1975).
[17] C.D. Chang, W.K. Bell, UK Patent 2,093,365 (1982).
[18] L.H. Slaugh, US Patent 4,375,424 (1983).
[19] T. Saita, K. Sangaya, Y. Seiko, Japan Patent 58 162 543 (1983).
[20] A. Shov, J.R. Rostrop-Nielsen, US Patent 4,520,216 (1985).
[21] M. Koike, T. Suzuki, K. Munemura, Japan Patent 60 179 494 (1985).
[22] C.-L. Sun, G.-Y. Cai, L.-L. Yi, China Patent1087033A (1992) (in Chinese).
[23] G.-Y. Cai, R.-M. Shi, Z.-Q. Jiang, China Patent1085824A (1992) (in Chinese).
[24] J.-S. Chen, C.-F. Wang, China Patent 1090222A, China Patent 1092760 (1993) (in Chinese).
[25] Z.-Y. Hou, J.-H, Fei, G.-X. Qi, X.-M. Zheng. J. Ind. Chem., submitted for publication.
[26] G.C. Chinchen, C.M. Hay, H.D. Vandervell, K.C. Waugh, J. Catal. 103 (1987) 79.
[27] J.B. Friedrich, M.S. Wainwaight, D.J. Young, J. Catal. 80 (1983) 1.
[28] J.W. Evans, M.S. Wainwaight, A.J. Bridgewater, D.J. Young, Appl. Catal. 7 (1983) 75.
[29] G.C. Chinchen, K.C. Waugh, D.A. Whan, Appl. Catal. 25 (1986) 101.
[30] B. Denise, R.P.A. Sneeden, B. Beguin, O. Cherifi, Appl. Catal. 30 (1987) 353.
[31] G.C. Chinchen, K.C. Waugh, J. Catal. 97 (1986) 280.

[32] T.H. Fleisch, R.L. Mieville, J. Catal. 90 (1984) 165.
[33] K. Klier, V. Chatikavanij, R.G. Herman, G.W. Simmons, J. Catal. 74 (1982) 343.
[34] R. Burch, R.J. Chappel, Appl. Catal. 45 (1992) 65.
[35] H. Berndt, V. Briehn, S. Evert, Appl. Catal. B86 (1992) 65.
[36] R.G. Herman, K. Klier, G. Simmons, B.P. Finn, J.W. Bulko, T.P. Kobylinski, J. Catal. 56 (1979) 407.
[37] S. Mehta, G.W. Simmons, K. Klier, R.G. Herman, J. Catal. 57 (1979) 339.
[38] R.M. Friedman, J.J. Freeman, F.W. Lytle, J. Catal. 55 (1978) 10.
[39] A. Wollner, F. Lange, Appl. Catal. 94 (1993) 181.
[40] J.F. Edwards, G.L. Schrader, J. Catal. 94 (1985) 175.
[41] J.F. Edwards, G.L. Schrader, J. Phys. Chem. 88 (1984) 5620.
[42] J.F. Edwards, G.L. Schrader, Appl. Spectrosc. 35 (1981) 559.